Philosophical Magazine,
Vol. 86, Nos. 33–35, 21 Nov.–11 Dec. 2006, 5497–5504

Taylor & Francis
Taylor & Francis Group

Using the instrumented indentation technique for stress characterization of friction stir-welded API X80 steel

Y. LEE†, J.-Y. KIM*‡, J.-S. LEE‡,
K.-H. KIM§, J. Y. KOO¶ and D. KWON‡

†Korea Research Institute of Standards and Science (KRISS),
Daejeon 305-340, Korea
‡Seoul National University, Seoul 151-744, Korea
§Frontics Inc., Seoul 151-744, Korea
¶ExxonMobil Research and Engineering Company,
New Jersey 08801, USA

(*Received 27 October 2005; in final form 27 April 2006*)

An instrumented indentation technique (IIT) appears to be a promising alternative to conventional stress measurement methods, particularly for welds with rapid microstructural gradients, because it has high spatial resolution and is non-destructive. The technique is used to characterize the residual stress of a friction stir-welded joint of API X80 steel. The indentation load–depth curve is significantly affected by the presence of residual stress and the stress-induced load change at a given penetration is converted to a quantitative stress value through an analytical model. All indentation test results show good agreement with those from an energy-dispersive X-ray diffraction performed to assess the validity of the IIT. In addition, the microstructures in various regions of the friction stir-welded joint and their effects on local microhardness are discussed.

1. Introduction

Residual stresses caused by inhomogeneous thermal and mechanical loads during welding affect subsequent fracture and fatigue behaviour, stress-corrosion cracking, and the like [1, 2]. Thus, the quantitative measurement of welding residual stress is important for the safe use and economical maintenance of industrial structures and facilities. Over the last few decades, a number of non-destructive methods have been developed, such as X-ray diffraction, ultrasonic method, Barkhausen noise and neutron diffraction, which are based on the relationship between the physical or crystallographic parameters and the residual stress [1]. Since the stress-sensitive parameters are, however, highly sensitive to metallurgical factors as well, applying these techniques to welded joints with rapid microstructural gradients is very difficult.

Thus, an indentation technique that allows almost non-destructive contact and is insensitive to environmental interferences has been suggested [3]. However, the initial

*Corresponding author. Email: juyoung1@snu.ac.kr

Philosophical Magazine
ISSN 1478–6435 print/ISSN 1478–6443 online © 2006 Taylor & Francis
http://www.tandf.co.uk/journals
DOI: 10.1080/14786430600776330

challenge was somewhat pointless because the alteration in hardness by the residual stress was less than 10% of its unstressed value. Recently, an instrumented indentation technique (IIT) that measures continuous deformation behaviour beneath an indenter as a curve of indentation load versus indenter penetration depth has been highlighted as an alternative to conventional mechanical tests [4–9]. This technique has many advantages, such as good data reproducibility, feasibility in in-field applications, a simple testing procedure and non-destructive characteristics. It has been used in previous studies to evaluate various mechanical properties such as hardness, elastic modulus [4, 5], yield strength, tensile strength, work-hardening index [6] and fracture toughness [7], and analysis procedures for plastic stress–strain response and hardness are currently being standardized [8, 9].

The stress sensitivity of the instrumented indentation curve and the application potential of this technique have been recognized by several researchers [10, 11]. However, most indentation studies for measuring stress have been tentative and somewhat empirical. Tsui *et al*. [12], studying the influence of in-plane stress on indentation plasticity by investigating both the shape of the indentation curve and the remnant contact impressions, reported that hardness was invariant regardless of the applied stress; this was supported by subsequent finite element analysis [13]. Suresh and Giannakopoulos [14] developed a theoretical model deriving a stress value from the ratio in contact area of stressed and unstressed materials by separating out a plastic deformation-related differential stress. However, hydrostatic stress still remained part of the differential contact stress, and the necessity of contact area observation for each indentation attenuates the convenience of the IIT. Thus, Lee and Kwon [15] developed another instrumented indentation model that quantified the residual stress by analyzing the surface stress effect on contact pressure in terms of shear plasticity. However, current theoretical models are difficult to apply to a general biaxial stress state because of their fundamental assumption of a simple equibiaxial stress state.

This study adapts Lee and Kwon's stress model [15] to a general biaxial stress state and uses this model to characterize a friction stir-welded API X80 steel by suggesting proper assumptions for the stress directionality and reference stress-free information. The residual stresses estimated are compared with those from an energy-dispersive X-ray diffraction technique. In addition, the influence of the characteristic microstructures in the friction stir-welded joint on local microhardness variation is discussed from a metallurgical viewpoint.

2. Theoretical models

2.1. *Model for a simple surface stress in an equibiaxial state*

A surface residual stress is assumed to be in an equibiaxial tensile state ($\sigma_{res,x}=\sigma_{res,y}=\sigma_{res}$, $\sigma_{res,z}=0$) and uniform in the near-surface region (taken as about three times the indentation depth) [14, 15]. If an arbitrary indentation state (h_t, L_0) is attained in an unstressed state and if the tensile in-plane stress, σ_{res}, is applied to the loading state at the fixed penetration depth, h_t, the indentation load, L_0,

will be reduced to a lower load, L_T, due to the decrease of surface penetration resistance. The load shift, $L_T - L_0$, due to the tensile stress application becomes a clue for stress quantification. The surface-normal deviator stress, σ_z^D, is $-2\sigma_{\text{res}}/3$ by removing the hydrostatic stress $2\sigma_{\text{res}}/3$from the surface residual stress, σ_{res}, and is added to the contact pressure [15]. $L_T - L_0$ is assumed to be the product of the selected deviator stress component and its corresponding contact area, A_C^T. Thus, an equation for the equibiaxial residual stress is derived in terms of the indentation load and contact area as:

$$\sigma_{\text{res}} = 3(L_0 - L_T)/\left(2A_C^T\right). \tag{1}$$

Here, A_C^T in the tensile stress state is calculated from $L_T A_C^0/L_0$ because the contact hardness, H or $L_0/A_C^0 = L_T/A_C^T$, is independent of the elastic residual stress. In order to measure the actual contact area, A_C^0, with pile-up or sink-in information from an Oliver–Pharr curve analysis [5], an empirical calibration for instrumental stiffness was performed through preliminary indentation tests on API X80 steel (see Lee and Kwon [16]).

2.2. *Model expansion for general welding stress in a biaxial state*

Since the experiments and theoretical models described above treat only equibiaxial residual stress, the magnitude of the average stress effect can be determined through the instrumented indentation technique but the directionality and magnitude of an actual biaxial stress cannot. This impedes wide application of the instrumented indentation technique to complex biaxial stress states in actual structures [17]. If we denote one major stress component of the biaxial residual stress as $\sigma_{\text{res},x}$ and the other as a minor stress component $\sigma_{\text{res},y}$, $\sigma_{\text{res},y}$ can be expressed as $\kappa\sigma_{\text{res},x}$ using the stress ratio κ, i.e. $\sigma_{\text{res},y}/\sigma_{\text{res},x}$. The influence of biaxial stress on the indentation plasticity also can be analyzed through a similar hydrostatic stress removal method. The deformation-sensitive deviator stress component is given as $\sigma_z^D = -(1+\kappa)\sigma_{\text{res},x}/3$ in this case. Thus, if information on κ is given, individual principal stresses can be calculated from the IIT using the following:

$$\sigma_{\text{res},x} = 3(L_0 - L_T)/\left((1+\kappa)A_C^T\right). \tag{2}$$

Note that equation (2) converges to equation (1), when a stress state approaches to the equibiaxial state or $\kappa = 1.0$.

Lee and Kwon [16] showed the validity of equation (2) by performing empirical indentation tests on biaxially strained specimens. The stress ratio became an important issue in stress characterization and a non-symmetrical contact deformation in uniaxial stress, observed by Underwood [18], supplied a clue for extracting the surface stress directionality. Lee *et al.* [19] tried to estimate the stress ratio by analyzing the pile-up heights along the two principal biaxial stress axes. The ratio of stress-induced pile-up shifts was linearly proportional to the stress ratio. Several preliminary observations on the welded joints yielded a stress ratio of about 0.33, and this value was used in subsequent biaxial stress analyses [20].

3. Experimental procedures

API X80 steel of thickness 20 mm was used in the friction stir-welding studies; its chemical composition (wt%) is 0.13 C, 1.52 Mn, 0.26 Si, 0.17 Mo, 0.034 Cr, 0.026 Ni, 0.0002 Nb, 0.003 Ti, 0.062 V, 0.041 Al, 0.032 Cu, 0.0003 B. Test plates were sectioned in half along the rolling direction and prepared for a butt joint. Oxide scale was removed by sand grinding followed by degreasing with methanol. An argon gas atmosphere was used to prevent oxidation during the weld cycle. Friction stir welding was done with a polycrystalline cubic boron nitride tool in an inert gas environment (MegaStir Technology, UT, USA); tool rotation and travel speeds were 550 rpm and 1.69 mm s^{-1}, respectively. Metallographic samples for optical observation, Vickers microhardness, instrumented indentation test (IIT) and energy-dispersive X-ray diffraction (ED-XRD) were prepared from the welded joint using metallographic procedures followed by etching with 2% nital solution. Vickers microhardness was probed using a 0.1 kg load across the welded joint.

A commercial AIS 3000R (Frontics, Inc., Seoul, Korea) with depth and load resolutions of 0.1 μm and 14.7 mN was used for the instrumented indentation tests, which were performed across the friction stir-welded joint at 2 mm intervals (a surface-parallel indentation testing array was made 2 mm from the welded surface). Two methods were used to obtain a reference indentation curve in a stress-free state corresponding to each microstructural region in the welds. The reference stress-free curve for the base metal, which underwent no microstructural change, was directly obtained from the remote base-metal region (about 10 mm from the welds) [21]. In addition, a multiple indentation method (5 kg load gap) was applied to characterize contact properties at several depth steps. The reference stress-free curve for the welding zone, which underwent significant microstructural change, was calculated through a unique analysis. The maximum applied load and testing speed were 50 kg and 0.3 mm min^{-1}, respectively. We used ED-XRD with a high-energy white beam synchrotron radiation source. The profiling was performed with the aid of highly collimated incident and scattered X-ray beams and with micropositioning of the sample surface. The profiling depth can attain the order of mm, and can be controlled with resolution of a few microns by radiation energy. When obtaining strain measurements using ED-XRD, we focused the depth at about 100 μm, similar to maximum indentation depth, to avoid any depth-difference effects between IIT and ED-XRD.

4. Results and discussion

4.1. *Microstructural variation and hardness distribution in the welded joint*

Figure 1 shows a macro image of the sectioned API X80 steel welds in which four distinctive microstructural regions can be identified from optical contrast differences. The corresponding microhardness variation is shown in figure 2. Whole microstructures in the welded joint had microhardness levels approximately similar to or

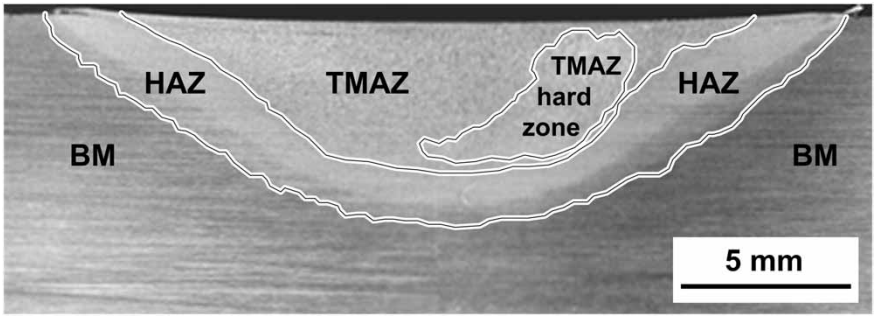

Figure 1. Four distinctive microstructural regions within the friction stir-welded API X80 steel.

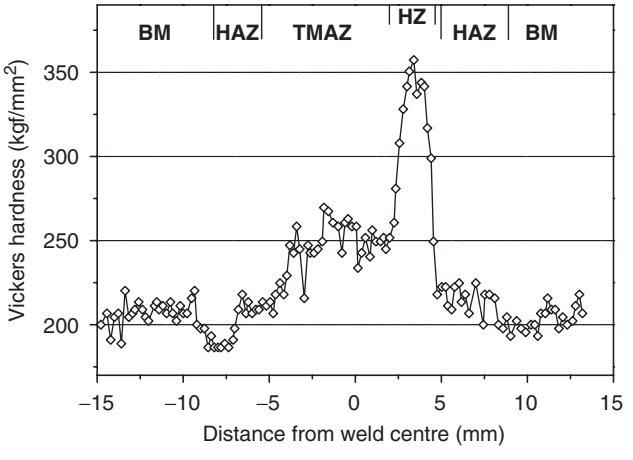

Figure 2. Microhardness distribution across the friction stir-welded joint.

higher than those of the base metal (BM), 180–210 kg mm^{-2}. In particular, a region located near the advancing side in the thermomechanically affected zone (TMAZ) had microhardness above 300 kg mm^{-2}. The presence of a hard zone (TMAZ-HZ in figure 2) and the gradual hardening behaviour from BM to TMAZ can be explained by microstructural change. The microstructure of API X80 steel, the base metal in this study, is composed of ferrite, granular bainite and martensite and its average grain size is about 7 μm. The existence of fine ($\leq$100 nm) globular Nb,Ti(C,N) precipitates has also been reported by Bangaru *et al*. [22]. The microstructure of the heat-affected zone (HAZ) was nearly the same as that of the BM except for a slight grain refinement (the average grain size of the HAZ was about 5 μm). The microstructure of TMAZ was a mixture of granular bainite, degenerate upper bainite and lath martensite, and its grain was highly coarsened to about 15 μm.

Although the average grain size increases over that in the BM and HAZ, the mixture of high-hardness phases increases the hardness of the TMAZ. The more dense acicular phases observed in the large TMAZ-HZ grain (about 30 μm) explains the significant hardness increment (see figure 2).

4.2. *Residual stress distributions across the friction stir-welded joint*

The instrumented indentation curves of the BM near the HAZ (solid triangles) and the reference curve for API X80 steel are presented together in figure 3. The load decrease due to surface stress at a given indentation depth means that the residual stress is of positive sign (tensile). By inserting $\kappa = 0.33$ into equation (2), the quantitative stress distribution inside the base metal was calculated, as plotted in figure 4. The BM reference indentation curve in figure 3 can be roughly fitted to $L = \alpha_B h^2$, where α_B is a hardness-proportional parameter (about upper 70% of the experimental solid line is fitted and overlapped in figure 3 as open triangles). The approximate reference indentation curves for the HAZ, TMAZ and TMAZ-HZ can also be fitted by calculating corresponding α values. For example, α_{TMAZ} in the TMAZ is calculated from $\alpha_B H_{\mathrm{TMAZ}}/H_B$. The selected indentation point was about 2 mm from the weld centre.The hardness ratio of the TMAZ and BM, H_{TMAZ}/H_B, was about 1.21 and thus α_{TMAZ} was $7.76 \times 10^9\,\mathrm{kg\,m^{-2}}$ when α_B for the BM was given as $6.41 \times 10^9\,\mathrm{kg\,m^{-2}}$.

Since the remnant indent morphologies from BM and other microstructures were very similar in this study, regardless of their different indent sizes, the α value could be compared directly. If remnant indents from two materials for the α

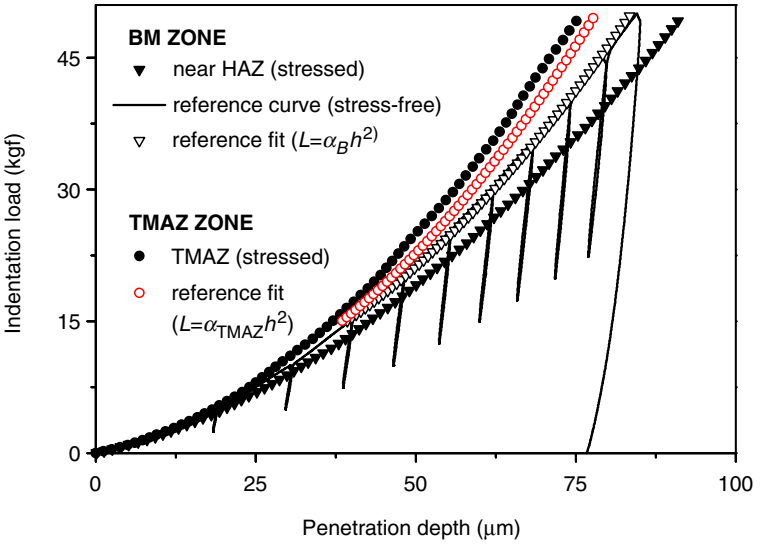

Figure 3. Experimental indentation curves (solid triangles and circles) from the welded joint in residual stress state and analytical reference curves (open triangles and circles) in stress-free state.

comparison have no geometrical similarity (i.e. two indents have different convexity around the contact periphery), this geometrical discrepancy must be considered in determining the α value for predicting proper shape of the loading curve.

The reference indentation curve calculated for the TMAZ is also plotted in figure 3 as open circles. Superposing the stressed indentation data and the newly calculated reference stress-free curve of the TMAZ, respectively, solid and open circles in figure 3 makes it possible to calculate a quantitative stress distribution in the TMAZ region. The stress distributions in the HAZ and TMAZ-HZ were also estimated by performing similar procedures. Finally the whole stress distribution of the friction stir-welded joint is plotted in figure 4 (solid circles). The residual stress profile measured from ED-XRD is also plotted in figure 4 (open circles). Except for the slight negative shift of the ED-XRD results (less than 50 MPa), the residual stress distributions from the IIT and ED-XRD were consistent throughout the whole welded joint. The discrepancy can be attributed to the indirectly calculated reference indentation curve and approximately determined stress ratio. The maximum tensile residual stress, about 150 MPa, was estimated near the BM-HAZ boundary, meaning that the BM-HAZ boundary is vulnerable to external loads. In addition, the high microhardness in the TMAZ-HZ region can be partially explained by the high compressive stress caused by the complex thermal cycle and phase transformation during the friction stir welding.

These experimental results suggest that the instrumented indentation technique is a promising non-destructive stress-measurement technique, especially for welded joints. However, the sparse indentation results, i.e. the 2 mm gap preventing the deformation field overlap, should be improved for more local welds by adopting such indentation techniques as zigzag probing.

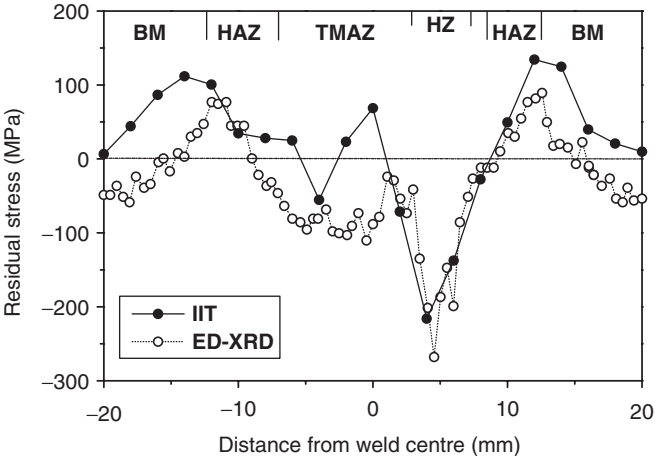

Figure 4. Residual stress distributions measured from the instrumented indentation technique (IIT) and energy dispersive X-ray diffraction.

5. Conclusions

Local variations in microstructure, hardness, and residual stress were explored using the microhardness and instrumented indentation techniques for friction stir-welded API X80 steel. Four distinctive microstructural regions were observed in the optically etched macro image. Comparing to the relatively fine grains (about 5–7 μm) in the heat-affected zone and base metal, the average grain sizes of the hard zone and its surrounding thermomechanically affected zone were about 30 and 15 μm, respectively. However, the microhardness in these microstructures showed a trend opposite to the grain size because the grains in the thermomechanically affected and hard zones contained dense, hard acicular phases. The residual stress profile assessed from the instrumented indentation technique showed high tensile stress (or compressive stress) near the base metal and heat-affected zone boundary (or near the thermomechanically affected zone–hard zone). Although there was a slight difference in quantitative value, the stress trend in instrumented indentation testing was perfectly consistent with the energy-dispersive X-ray diffraction results. Thus the instrumented indentation technique is a promising stress-measurement technique if its current limitations are handled successfully by reference indentation curve formation, stress ratio determination, and zigzag probing.

References

[1] J. Lu, M.R. James and G. Roy, in *Handbook of Measurement of Residual Stresses*, edited by J. Lu (Fairmont Press, Lilburn, GA, 1996).
[2] C.O. Ruud, P.S. DiMascio and J.J. Yavelak, Expl Mech. **25** 338 (1985).
[3] G. Sines and R. Carlson, ASTM Bull. **180** 35 (1952).
[4] M.F. Doerner and W.D. Nix, J. Mater. Res. **1** 601 (1986).
[5] W.C. Oliver and G.M. Pharr, J. Mater. Res. **7** 1580 (1992).
[6] J.-H. Ahn and D. Kwon, J. Mater. Res. **16** 3170 (2001).
[7] Y.-H. Lee and D. Kwon, Key Engng Mater. **161–163** 569 (1999).
[8] KS (Korean Standards) B 0950: Metallic materials – Instrumented indentation test for indentation tensile properties (07-Nov-2002).
[9] ISO (International Organization for Standardization) 14577: Metallic materials – Instrumented indentation test for hardness and materials parameters (10-Oct-2002).
[10] W.R. LaFontaine, C.A. Paszkiet, M.A. Korhonen, *et al*., J. Mater. Res. **6** 2084 (1991).
[11] A.V. Zagrebelny and C.B. Carter, Scripta Mater. **37** 1869 (1997).
[12] T.Y. Tsui, W.C. Oliver and G.M. Pharr, J. Mater. Res. **11** 752 (1996).
[13] A. Bolshakov, W.C. Oliver and G.M. Pharr, J. Mater. Res. **11** 760 (1996).
[14] S. Suresh and A.E. Giannakopoulos, Acta Mater. **46** 5755 (1998).
[15] Y.-H. Lee and D. Kwon, Scripta Mater. **49** 459 (2003).
[16] Y.-H. Lee and D. Kwon, Acta Mater. **52** 1555 (2004).
[17] A.E. Giannakopoulos, J. Appl. Mech. **70** 638 (2003).
[18] J.H. Underwood, Expl Mech. **13** 373 (1973).
[19] Y.-H. Lee, K. Takashima, Y. Higo, *et al*., Scripta Mater. **51** 887 (2004).
[20] Y. Choi, Y.-H. Lee, J.-I. Jang, *et al*., Key Engng Mater. **297–300** 2122 (2005).
[21] Y.-H. Lee, D. Kwon, J.-I. Jang, *et al*., Key Engng Mater. **270–273** 35 (2004).
[22] N.V. Bangaru, D.P. Fairchid, M.L. Macia, *et al*., paper presented at the 4th International Conference on Pipeline Technology, Ostend, 9–13 May (2004).